The 2013 World Congress on
Advances in Structural Engineering and Mechanics (ASEM13)
Jeju, Korea, September 8-12, 2013

Numerical Analysis of Hybrid Substructure with Multi-cylinders for Wind Turbines

*Min-Su Park[1)], Youn-Ju Jeong[2)] and Young-Jun You[3)]

[1), 2), 3)] *Structural Engineering Research Division, Korea Institute of Construction Technology, Goyang-Si 411-712, Korea*
[1)] *mspark@kict.re.kr*

ABSTRACT

For the reliable design of substructure supporting wind turbines it is very important to reduce the effects of wave forces. In the present study, the hybrid substructure with multi-cylinders is newly suggested to reduce the effect of wave forces. Using diffraction theory the scattering wave in a fluid region is expressed by an Eigen-function expansion method to calculate the wave force acting on the hybrid substructure. The wave force and wave run-up acting on the hybrid substructure is presented to examine the water wave interaction according to the variation of circular cylindrical size and the distance among cylinders. It is found that the hybrid substructure with multi-cylinders is very useful to reduce the effect of wave forces acting on the substructure.

1. INTRODUCTION

Since the size of a tower and a rotor-nacelle becomes larger with increment of wind turbine's gross generation, the size of a substructure supporting wind turbines is gradually increased. In other words, the substructure is strongly influenced by the effect of wave forces as the size of substructure increases. Therefore, it is very import to reduce the wave force acting on substructures. In the present study the hybrid substructure, which is composed of multi-cylinders having different radius of each upper and lower area shown in Fig. 1, is newly suggested to reduce the wave forces.

The water wave interaction with multi-cylinders has been studied by many researchers. Under the assumption of potential flow and linear wave theory, Spring and Monkmeyer (1974) first proposed a semi-analytical solution for impermeable cylinders using an Eigen-function expansion approach. In the case of N bottom-mounted circular cylinders Linton and Evans (1990) simplified this solution. Kagemoto and Yue (1986) developed another exact solution within the context of linearized theory, showing that a

[1), 3)] Senior Researcher
[2)] Research Fellow

general three-dimensional wave diffraction problem could be solved in terms of algebraically-based diffraction characteristics of a single member. Another popular approach based on the wide-spacing assumption was the modified plane wave method, developed by McIver and Evans (1984). This approach was later applied to a variety of cases by McIver (1984), Williams and Demirbilek (1988), Williams and Abul-Azm (1989), and Williams and Rangappa (1994). For the analysis of N full-body porous-surfaced cylinders, the Eigen-function expansion method could also be employed to describe hydrodynamic interactions in multi-bodied structures (Williams and Li 1998, 2000; Cho and Kim 2010; Park et al. 2010; Zhao et al. 2011).

In the present study, the fluid domain is divided into two regions: an interior region and an exterior region. Using diffraction theory the scattering wave in each fluid region is expressed by an Eigen-function expansion method with using three-dimensional linear potential theory to calculate the wave force acting on the hybrid substructure with multi-cylinders. The comparison of wave forces and wave run-ups is made for the different depth ratio of interior region. In order to examine the water wave interaction with hybrid substructures the wave forces and the wave run-ups are presented for the different array of hybrid substructures with multi-cylinders.

2. FORMULATION

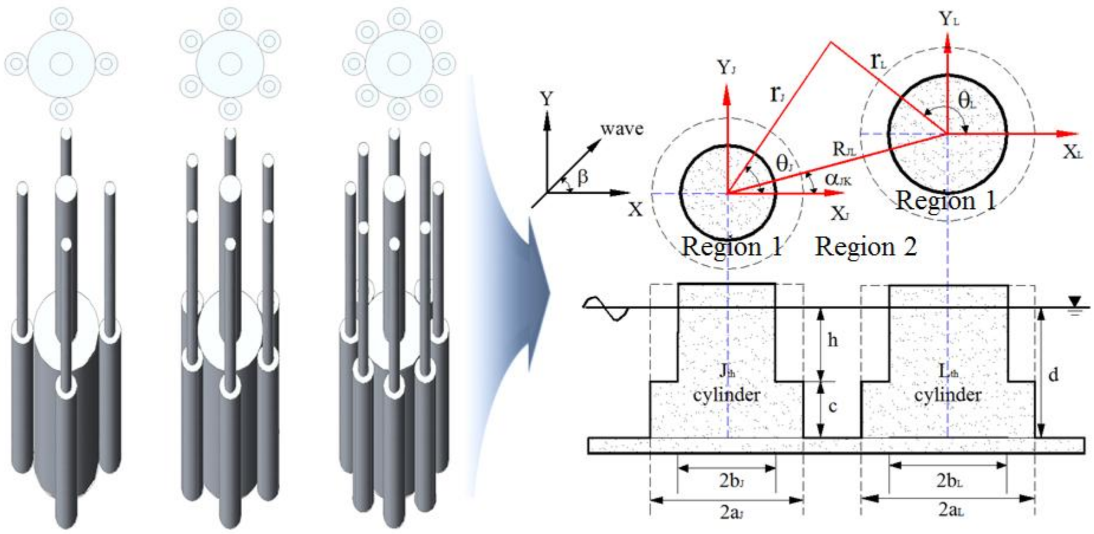

Fig. 1. Coordinate system for an array of hybrid substructures.

A hybrid substructure for wind turbines is composed of multi-cylinders having different radiuses of each upper and lower area shown in Fig. 1. The hybrid substructure is situated in water of uniform depth *d* and the draughts of each upper and lower area are *h* and *c*, respectively. The lower and the upper radius of the *j*th cylinder are a_j and b_j, respectively. Also, the global Cartesian coordinate system(x, y, z) is defined with an origin located on the sea bed with the z-axis directed vertically upwards. The center of each cylinder at (x_j, y_j) is taken as the origin of a local polar coordinate system (r_j, θ_j), where θ_j is measured counter-clockwise from the positive x-axis. The center of the *l*th cylinder has a polar coordinate (R_{jl}, α_{jl}) relative to the *j*th cylinder. The coordinate relationship between the *j*th and *l*th cylinder is shown in Fig. 1. Moreover, the fluid domain is divided into two regions: region 1 which is interior to the cylinder ($b_j \le r_j \le a_j$, $d-h \le z \le d$) and region 2 which is exterior to the cylinder and extends to infinity in the horizontal plane ($r_j \ge a_j$, $0 \le z \le d$).

It is assumed that the computational fluid domain is inviscid, and incompressible, and its motion is irrotational. The array of cylinders is subjected to a train of regular waves of height H and angular frequency ω propagating at an angle β to the positive x-axis. The velocity potential of the computational domain can be written as

$$\Phi(x,y,z,t) = \mathrm{Re}\left[-\{igH/(2\omega)\}\phi(x,y,z)e^{-i\omega t}\right] \tag{1}$$

where $\mathrm{Re}[\ ]$ denotes the real part of a complex velocity potential Φ , and g is the gravitational acceleration.

As a governing equation, the Laplace equation is satisfied for the entire fluid domain of the present boundary value problem:

$$\nabla^2\phi = 0 \tag{2}$$

For solving the governing equation, the following boundary conditions for the free surface (Eq. (3)), bottom of region 1 (Eq. (4)), vertical wall of upper and lower area (Eq. (5)), flat rigid sea bottom (Eq. (6)), and the Sommerfeld radiation boundaries (Eq. (7)) can be given, respectively:

$$\frac{\partial\phi}{\partial z} - \frac{\omega^2}{g}\phi = 0 \qquad on \quad z = d \tag{3}$$

$$\frac{\partial\phi}{\partial z} = 0 \qquad on \quad z = d-h,\ b_j \le r \le a_j \tag{4}$$

$$\frac{\partial\phi}{\partial r_j} = 0 \qquad \begin{array}{l} on \quad r = b_j,\ (d-h) \le z \le d \\ on \quad r = a_j,\ 0 \le z \le (d-h) \end{array} \tag{5}$$

$$\frac{\partial\phi}{\partial z} = 0 \qquad on \quad z = 0 \tag{6}$$

$$\lim_{r\to\infty}\sqrt{r}\left[\frac{\partial}{\partial r}(\phi_2 - \phi_{in}) - ik(\phi_2 - \phi_{in})\right] = 0 \tag{7}$$

where k is the incident wave number related to the wave frequency through the dispersion relation $\omega^2 = gk\tanh kd$, and d is the water depth. ϕ_2 and ϕ_{in} denote the total velocity potential in region 2 and the incident wave potential, respectively.

The wave potential in the interior region(1) of the jth cylinder, which satisfies the appropriate free surface and structural boundary conditions, can be expressed by the following Eigen-function expansion,

$$\phi_1^j = \sum_{n=-\infty}^{n=\infty} \left[A_n^j J_n\left(k_0 r_j\right) - \frac{J_n'\left(k_0 b_j\right)}{Y_n'\left(k_0 b_j\right)} A_n^j Y_n\left(k_0 r_j\right) \right] \times \frac{\cosh\left\{k_0\left(z-d+h\right)\right\}}{\cosh\left(k_0 h\right)} e^{in\theta_j} \quad (8)$$

in which J_n and Y_n denotes the Bessel function of the first and the second kind of order n, and J_n' and Y_n' are the first derivatives of the Bessel function, respectively. A_n^j is the unknown complex potential coefficient. A new wave number k_0 is introduced, which satisfies the dispersion relation $\omega^2 = gk_0 \tanh k_0 h$, where h denote local water depth in the interior region 1.

The incident wave potential in the jth local polar coordinate system can be expressed using Jacobi-Anger expansion of Bessel function as follows,

$$\phi_{in}^j = \frac{\cosh kz}{\cosh kd} T_j \sum_{n \to -\infty}^{\infty} J_n\left(kr_j\right) e^{in\left(\pi/2+\theta_j-\beta\right)} \quad (9)$$

where $T_j = e^{ik\left(x_j \cos\beta + y_j \sin\beta\right)}$ is a phase factor associated with the cylinder j from the global origin.

The wave potential in the exterior region (2), which is expressed by using Graf's addition theorem for the Bessel Functions (Abramowitz and Stegun, 1972) and satisfies the Helmholtz equation, can be expressed by the following Eigen-function expansion,

$$\phi_2^j\left(r_j,\theta_j\right) = \sum_{n=-\infty}^{n=\infty} \left[\begin{array}{l} e^{ik\left(x_j\cos\beta+y_j\sin\beta\right)} J_n\left(kr_j\right) e^{in\left(\pi/2-\beta\right)} \\ +C_n^j \dfrac{H_n\left(kr_j\right)}{H_n'\left(ka_j\right)} + \displaystyle\sum_{\substack{l=1 \\ l\neq j}}^{N} \sum_{m=-\infty}^{m=\infty} C_m^l \frac{a_l J_n\left(kr_j\right)}{a_j H_m'\left(ka_l\right)} H_{m-n}\left(kR_{lj}\right) e^{i(m-n)\alpha_{lj}} \end{array} \right] \times \frac{\cosh kz}{\cosh kd} e^{in\theta_j} \quad (10)$$

The right-hand side of Eq. (10) represents the incident wave upon the jth cylinder, the scattered wave produced by the jth cylinder, and the re-scattered wave generated by the adjacent cylinder l, respectively. C_n^j is the unknown complex potential coefficient. H_n is the Hankel function of first kind of order n, and H_n' is the first derivatives of the Hankel function, respectively.

In addition to applying the body boundary conditions associated with the free surface conditions, the present boundary value problem must satisfy the matching conditions at the interface between the regions, which are given by,

$$\begin{array}{l} \phi_1^j = \phi_2^j \quad on \quad r_j = a_j,\ d-h \le z \le d \\ \dfrac{\partial \phi_1^j}{\partial r} = \dfrac{\partial \phi_2^j}{\partial r} \quad on \quad r_j = a_j,\ d-h \le z \le d \end{array} \quad (11)$$

Substituting Eq. (8) and (10), and using the orthogonality of depth from $z=d-h$ to d, the first matching condition between region 1 and 2 in Eq. (11) can be rewritten as,

$$\sum_{n=-\infty}^{\infty} A_n^j \left\{ J_n\left(k_0 a_j\right) - \frac{J_n'\left(k_0 b_j\right)}{Y_n'\left(k_0 b_j\right)} Y_n\left(k_0 a_j\right) \right\} \int_{d-h}^{d} \left\{ \frac{\cosh\left\{k_0\left(z-d+h\right)\right\}}{\cosh\left(k_0 h\right)} \right\}^2 dz$$

$$= \sum_{n=-\infty}^{\infty} \left[\begin{array}{l} e^{ik\left(x_j \cos\beta + y_j \sin\beta\right)} J_n\left(ka_j\right) e^{in\left(\pi/2-\beta\right)} \\ +C_n^j \dfrac{H_n\left(ka_j\right)}{H_n'\left(ka_j\right)} + \displaystyle\sum_{\substack{l=1 \\ l\neq j}}^{N} \sum_{m=-\infty}^{m=\infty} C_m^l \dfrac{a_l J_n\left(ka_j\right)}{a_j H_m'\left(ka_j\right)} H_{m-n}\left(kR_{lj}\right) e^{i(m-n)\alpha_{lj}} \end{array} \right] \times \int_{d-h}^{d} \left\{ \frac{\cosh kz}{\cosh kd} \frac{\cosh\left\{k_0\left(z-d+h\right)\right\}}{\cosh\left(k_0 h\right)} \right\} dz \tag{12}$$

Applying the orthogonal property to the second matching conditions in Eq. (11), with respect to z over the region of validity, the following equation can be obtained:

$$\int_0^d \frac{\partial \phi_2^j}{\partial r} \left\{ \frac{\cosh kz}{\cos kd} \right\} dz = \int_0^{d-h} \frac{\partial \phi_2^j}{\partial r} \frac{\cosh kz}{\cos kd} dz + \int_{d-h}^{d} \frac{\partial \phi_1^j}{\partial r} \frac{\cosh kz}{\cos kd} dz \tag{13}$$

By applying Eq. (12) to Eq. (13), the key equation for unknown coefficients C_n^j can be obtained as follows,

$$C_n^j \left[\begin{array}{l} k\displaystyle\int_0^d \left\{ \frac{\cosh kz}{\cosh kd} \right\}^2 dz - \frac{\left\{ J_n'\left(k_0 a_j\right) - \dfrac{J_n'\left(k_0 b_j\right)}{Y_n'\left(k_0 b_j\right)} Y_n'\left(k_0 a_j\right) \right\} k_0}{\left\{ J_n\left(k_0 a_j\right) - \dfrac{J_n'\left(k_0 b_j\right)}{Y_n'\left(k_0 b_j\right)} Y_n\left(k_0 a_j\right) \right\}} \times \frac{H_n\left(ka_j\right)}{H_n'\left(ka_j\right)} H_n\left(ka_j\right) \\ \times \dfrac{\displaystyle\int_{d-h}^{d} \left\{ \frac{\cosh k_0\left(z-d+h\right)}{\cosh k_0 h} \frac{\cosh kz}{\cosh kd} \right\} dz \times \int_{d-h}^{d} \left\{ \frac{\cosh k_0\left(z-d+h\right)}{\cosh k_0 h} \frac{\cosh kz}{\cosh kd} \right\} dz}{\displaystyle\int_{d-h}^{d} \left\{ \frac{\cosh k_0\left(z-d+h\right)}{\cosh k_0 h} \right\}^2 dz} \end{array} \right]$$

$$+\sum_{\substack{l=1 \\ l=j}}^{N} \sum_{m=-\infty}^{m=\infty} C_m^l \frac{a_l H_{m-n}\left(kR_{lj}\right)}{a_j H_m'\left(ka_l\right)} e^{i(m-n)\alpha_{lj}} \left[\begin{array}{l} J_n'\left(ka_j\right) k\displaystyle\int_0^d \left\{ \frac{\cosh kz}{\cosh kd} \right\}^2 dz - \frac{\left\{ J_n'\left(k_0 a_j\right) - \dfrac{J_n'\left(k_0 b_j\right)}{Y_n'\left(k_0 b_j\right)} Y_n'\left(k_0 a_j\right) \right\} k_0}{\left\{ J_n\left(k_0 a_j\right) - \dfrac{J_n'\left(k_0 b_j\right)}{Y_n'\left(k_0 b_j\right)} Y_n\left(k_0 a_j\right) \right\}} J_n\left(ka_j\right) \\ \times \dfrac{\displaystyle\int_{d-h}^{d} \left\{ \frac{\cosh k_0\left(z-d+h\right)}{\cosh k_0 h} \frac{\cosh kz}{\cosh kd} \right\} dz \times \int_{d-h}^{d} \left\{ \frac{\cosh k_0\left(z-d+h\right)}{\cosh k_0 h} \frac{\cosh kz}{\cosh kd} \right\} dz}{\displaystyle\int_{d-h}^{d} \left\{ \frac{\cosh k_0\left(z-d+h\right)}{\cosh k_0 h} \right\}^2 dz} \end{array} \right]$$

$$
=-e^{ik\left(x_j\cos\beta+y_j\sin\beta\right)}e^{in\left(\pi/2-\beta\right)}\left[\begin{array}{l} J_n'\left(ka_j\right)k\int_0^d\left\{\frac{\cosh kz}{\cosh kd}\right\}^2dz-\frac{\left\{J_n'\left(k_0a_j\right)-\frac{J_n'\left(k_0b_j\right)}{Y_n'\left(k_0b_j\right)}Y_n'\left(k_0a_j\right)\right\}k_0}{\left\{J_n\left(k_0a_j\right)-\frac{J_n'\left(k_0b_j\right)}{Y_n'\left(k_0b_j\right)}Y_n\left(k_0a_j\right)\right\}}J_n\left(ka_j\right) \\ \times\frac{\int_{d-h}^d\left\{\frac{\cosh k_0\left(z-d+h\right)}{\cosh k_0h}\frac{\cosh kz}{\cosh kd}\right\}dz\times\int_{d-h}^d\left\{\frac{\cosh k_0\left(z-d+h\right)}{\cosh k_0h}\frac{\cosh kz}{\cosh kd}\right\}dz}{\int_{d-h}^d\left\{\frac{\cosh k_0\left(z-d+h\right)}{\cosh k_0h}\right\}^2dz}\end{array}\right] \qquad (14)
$$

In order to calculate the potential coefficients C_n^j from the infinite system, Eq. (14) is truncated to *(2M+1)N* equations with *(2M+1)N* unknown values for *j=1, 2,…, N* and *n=-M,…, M*. That is,

$$
\begin{aligned}
&C_n^j\left\{kS_1-\frac{Q_1k_0S_2}{Q_2S_3}\frac{H_n\left(ka_j\right)}{H_n'\left(ka_j\right)}H_n\left(ka\right)\right\}\\
&+\sum_{\substack{l=1\\l=j}}^{N}\sum_{m=-M}^{m=M}C_m^l\frac{a_lH_{m-n}\left(kR_{lj}\right)}{a_jH_m'\left(ka_l\right)}e^{i(m-n)\alpha_{lj}}\left\{J_n'\left(ka_j\right)kS_1-\frac{Q_1k_0S_2}{Q_2S_3}J_n\left(ka_j\right)\right\}\\
&=-e^{ik\left(x_j\cos\beta+y_j\sin\beta\right)}e^{in\left(\pi/2-\beta\right)}\left\{J_n'\left(ka_j\right)kS_1-\frac{Q_1k_0S_2}{Q_2S_3}J_n\left(ka_j\right)\right\}
\end{aligned} \qquad (15)
$$

where,

$$S_1=\int_0^d\left\{\frac{\cosh kz}{\cosh kd}\right\}^2dz$$

$$S_2=\int_{d-h}^d\left\{\frac{\cosh k_0\left(z-d+h\right)}{\cosh k_0h}\frac{\cosh kz}{\cosh kd}\right\}dz\times\int_{d-h}^d\left\{\frac{\cosh k_0\left(z-d+h\right)}{\cosh k_0h}\frac{\cosh kz}{\cosh kd}\right\}dz$$

$$S_3=\int_{d-h}^d\left\{\frac{\cosh k_0\left(z-d+h\right)}{\cosh k_0h}\right\}^2dz$$

$$Q_1=\left\{J_n'\left(k_0a_j\right)-\frac{J_n'\left(k_0b_j\right)}{Y_n'\left(k_0b_j\right)}Y_n'\left(k_0a_j\right)\right\}$$

$$Q_2=\left\{J_n\left(k_0a_j\right)-\frac{J_n'\left(k_0b_j\right)}{Y_n'\left(k_0b_j\right)}Y_n\left(k_0a_j\right)\right\}$$

By using a stand matrix technique, the equations on C_n^j can be solved and the unknown coefficients A_n^j may then be obtain from Eq. (12) by applying C_n^j. In this manner the velocity potential in each fluid region (ϕ_1^j , ϕ_2^j) can be determined. After solving the velocity potentials, the wave excitation forces on each cylinder are obtained using the integration of pressure on the wetted surface of cylinder. Wave forces in x-direction (F_x) and in y-direction (F_y) are calculated as follows,

$$F_x^j = -i\rho\omega\int_{d-h}^{d}\int_0^{2\pi}\frac{-igH}{2\omega}\left\{\phi_1^j\right\}b_j\cos\theta d\theta dz \quad on \quad d-h\le z\le d$$
$$F_y^j = -i\rho\omega\int_{d-h}^{d}\int_0^{2\pi}\frac{-igH}{2\omega}\left\{\phi_1^j\right\}b_j\sin\theta d\theta dz \quad on \quad d-h\le z\le d \tag{16}$$

$$F_x^j = -i\rho\omega\int_0^{d-h}\int_0^{2\pi}\frac{-igH}{2\omega}\left\{\phi_2^j\right\}a_j\cos\theta d\theta dz \quad on \quad 0\le z\le d-h$$
$$F_y^j = -i\rho\omega\int_0^{d-h}\int_0^{2\pi}\frac{-igH}{2\omega}\left\{\phi_2^j\right\}a_j\sin\theta d\theta dz \quad on \quad 0\le z\le d-h \tag{17}$$

where Eq. (16) is for upper part and Eq. (17) is for lower part of the hybrid substructure with multi-cylinders.

3. NUMERICAL RESULTS AND DISCUSSION

In order to verify the wave forces on an array of four cylinders, the present numerical results are compared with the numerical results of Williams and Li (2000) for the various incident wave angles. The wave forces are normalized by $\rho g(H/2)a_1^2$ and the axis of abscissa denotes the wave number. The calculated wave forces are in good agreement with the results from Williams and Li (2000) shown in Fig. 2.

Fig. 3 show the comparison of wave forces on hybrid substructure with five cylinders for various depths(h/d) of region 1. The calculation conditions are a_1=3.0m, b_1=1.0m, a_j=1.0m, b_j=0.5m (j=2,3,4,5) and d=20.0m. The large cylinder 1 is located at (0, 0)m, and the other cylinders are numbered clockwise from 2 to 5 and situated at (-4, 0)m, (0, -4)m, (4, 0)m, and (0, -4)m, respectively. In the comparison the ratio of h/d=0.0 indicates the case without small cylinders of region 1, while h/d=1.0 represents the case with only small cylinders. The calculated total wave forces are normalized by $\rho g(H/2)a_1^2$. In the comparison, the peak wave force with depth 0.25 and 0.5 decreases about 33% and 50%, respectively, compared to the peak value of depth 1.0. Although in the long wave region (ka≤0.8) the pattern of wave forces is strongly influenced by the depth of region 1, the pattern of both depth 0.5 and 0.0 becomes very similar, and the difference between depth 0.5 and 0.0 is very small in the short wave region (ka≥0.8). The wave forces on the hybrid substructure with the depth 0.25 become remarkably smaller than that on mono pile as the wave number becomes larger than 0.6. It means that the hybrid substructure with depth 0.25 of region 1 is significantly efficient to reduce the wave forces acting on hybrid substructures in the short wave region.

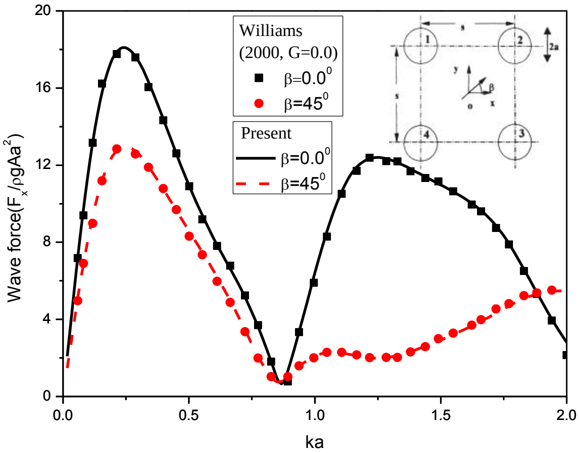

Fig. 2. Comparison of wave forces in x-direction on the array of four cylinders with Williams and Li(2000) for d/*a*=5, s/*a*=4

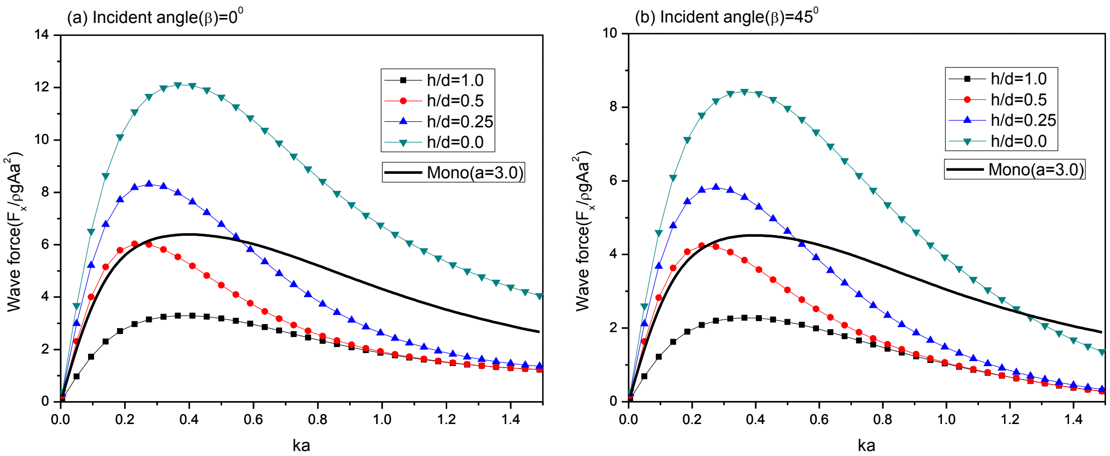

Fig. 3. Comparison of total wave forces on the hybrid substructure of five cylinders with a_1=3.0m, b_1=1.0m, a_j=1.0m, b_j=0.5m (j=2,3,4,5) and d=20.0m for various depths (h): (a) x-direction for β=0.0^0, (b) x-direction for β=45.0^0

The wave forces on each cylinder of the hybrid substructure with five cylinders are presented in Fig. 4. In case of incident wave angle 0.0^0 the wave forces on cylinder 1 are largest and the wave forces on cylinder 3 and 5 have same values. The pattern of cylinder 3 and 5 in x-direction shows the same pattern of cylinder 4 and 2 in y-direction in case of incident wave angle 45^0.

Fig. 5 shows the comparison of total wave forces on the hybrid substructure with five cylinders for various radiuses (b_1) of cylinder 1. Since the wave force is closely related to the wetted surface of structure, the wave forces gradually decrease as the radius of cylinder1 decreases. The hybrid substructure with the radius less than 0.2 is significantly efficient to reduce the wave forces in short wave region(ka≥0.6) compared to the substructure with mono pile.

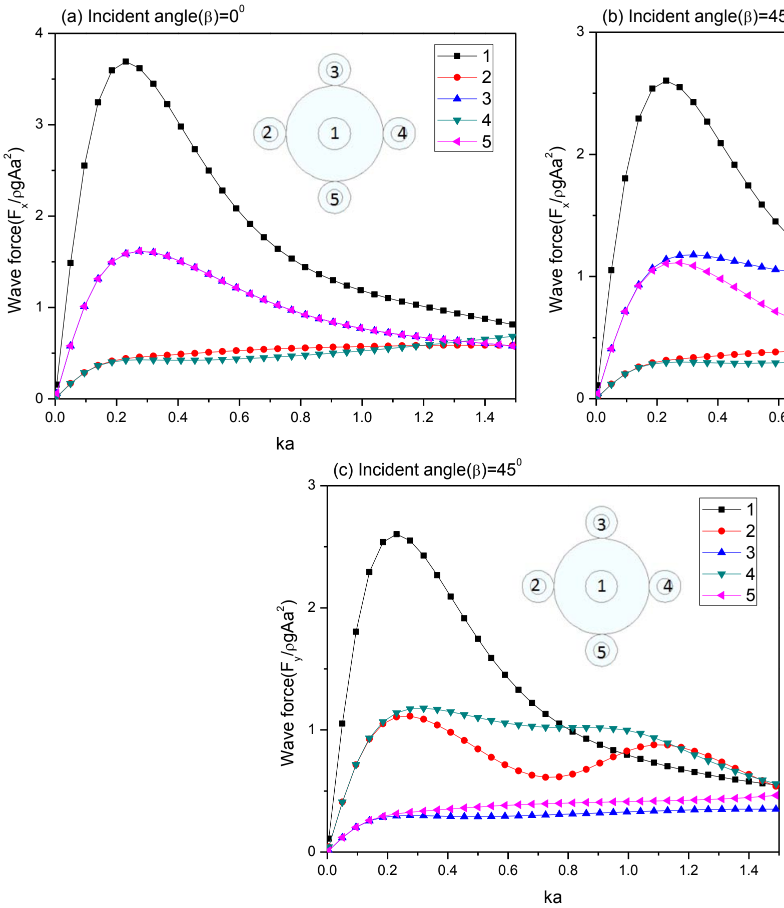

Fig. 4. Comparison of wave forces on each cylinder with a_1=3.0m, b_1=1.0m, a_j=1.0m, b_j=0.5m(j=2,3,4,5) and d=20.0m for various incident wave angles (β): (a) x-direction for β=0.0^0, (b) x-direction for β=45.0^0, (c) y-direction for β=45.0^0

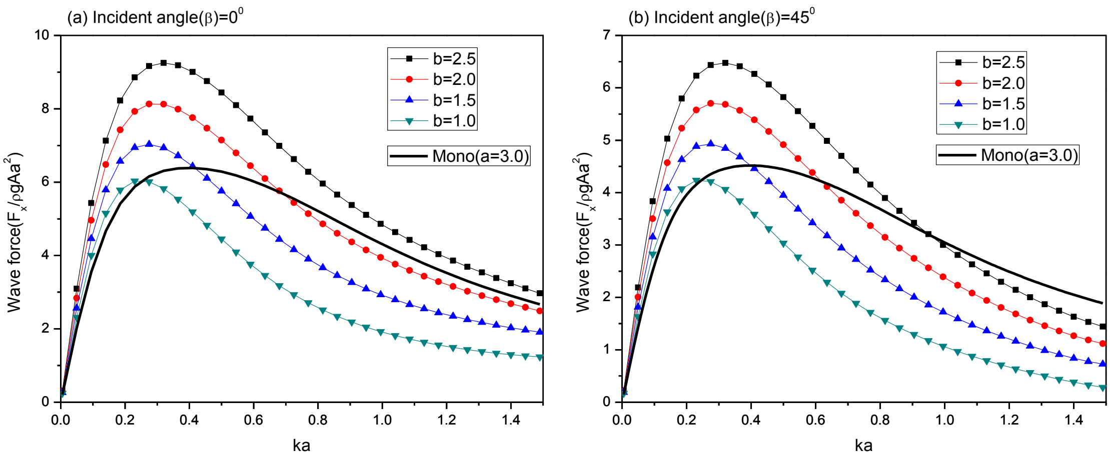

Fig. 5. Comparison of total wave forces on the hybrid substructure of five cylinders with a_1=3.0m, a_j=1.0m, b_j=0.5m(j=2,3,…,5) and d=20.0m for various radiuses of cylinder 1 (b_1): (a) x-direction for β=0.0^0, (b) x-direction for β=45.0^0

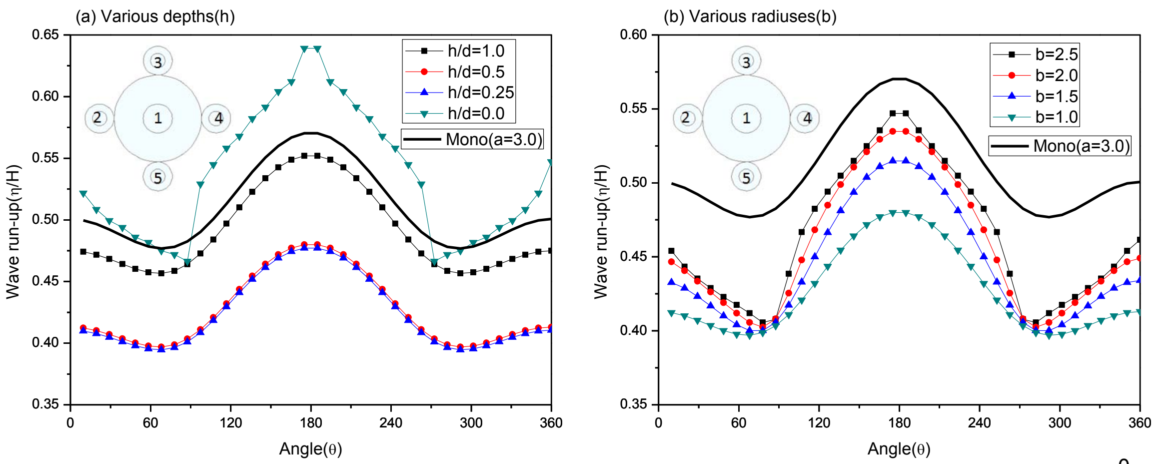

Fig. 6. Comparison of wave run-ups on cylinder 1 for five cylinders with β=0.0^0 and ka=0.3: (a) Various depths(h), (b) Various radiuses(b)

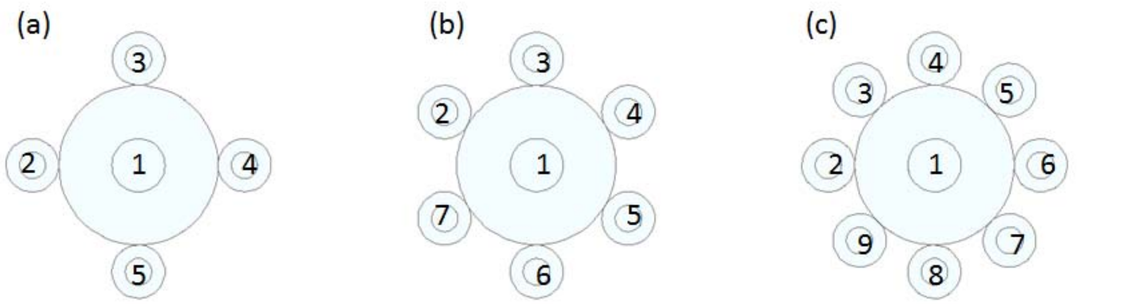

Fig. 7. Hybrid substructure: (a) Five cylinders, (b) Seven cylinders, (c) Nine cylinders

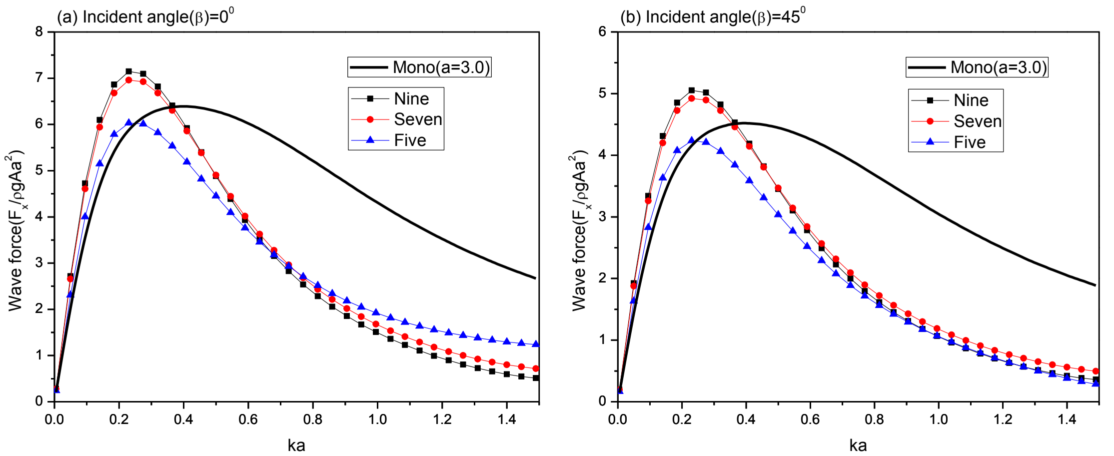

Fig. 8. Comparison of total wave forces on the hybrid substructure of various cylinder numbers with a_1=3.0m, b_1=1.0m, a_j=1.0m, b_j=0.5m(j=2,3,…,7) and d=20.0m for various incident wave angles (β): (a) x-direction for β=0.0^0, (b) x-direction for β=45.0^0

Fig. 6 shows the comparison of wave run-up on cylinder 1 for five cylinders with the incident wave angle(β) 0.0^0. Since the wave force has the peak value when the wave number is 0.3, the comparison of wave run-up is made for the wave number 0.3. The wave run-up is normalized by incident wave height (H) and the abscissa denotes the angle(θ) measured counterclockwise from the positive x-axis. The wave run-up on cylinder 1 is largest when the depth of region 1 is 0.0. However, in case of depth 1.0 with only small cylinders the wave run-up is smaller than that of depth 1.0 and mono pile. Although the difference of wave run-up between the depth 0.25 and 0.5 is small, the wave run-up on hybrid substructure is smallest for all cases. It means that the hybrid substructure remarkably reduce the wave run-up on cylinder 1.

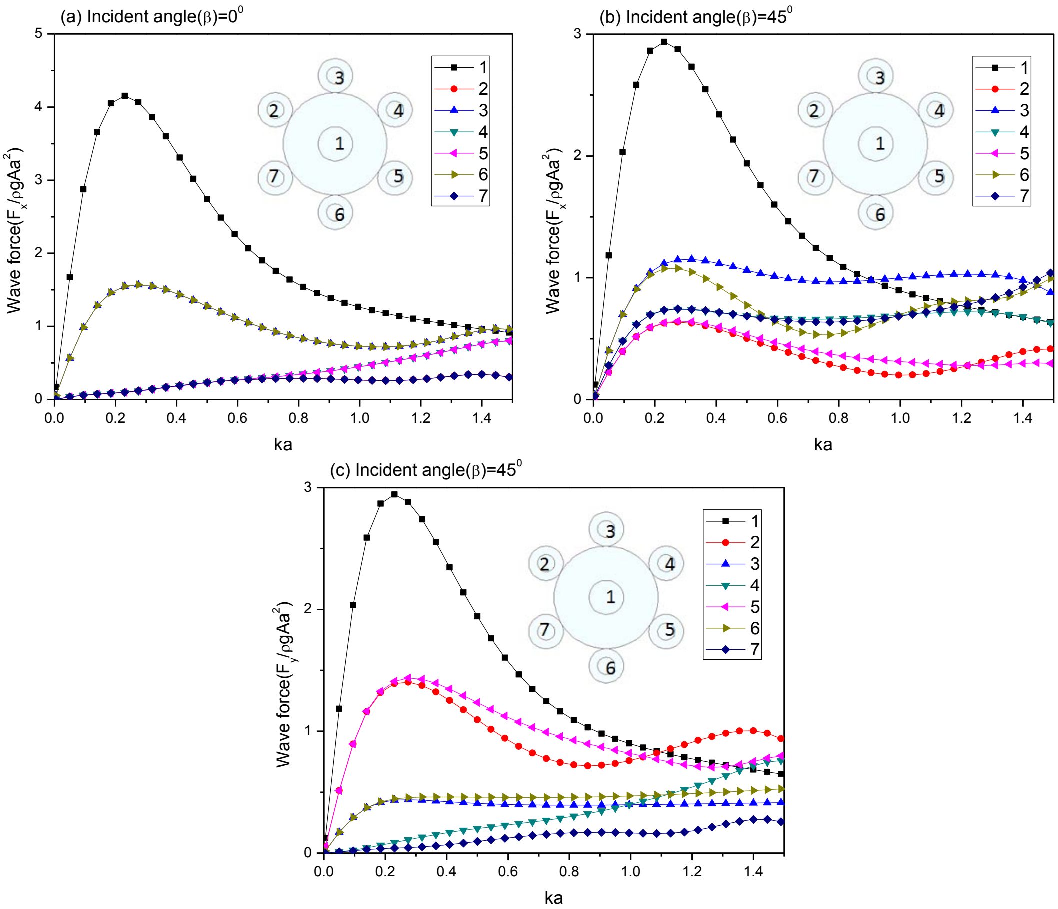

Fig. 9. Comparison of wave forces on each cylinder with a_1=3.0m, b_1=1.0m, a_j=1.0m, b_j=0.5m(j=2,3,…,7) and d=20.0m for various incident wave angles (β): (a) x-direction for $\beta=0.0^0$, (b) x-direction for $\beta=45.0^0$, (c) y-direction for $\beta=45.0^0$

The Comparison of total wave forces on the hybrid substructure of various cylinder numbers is presented in Fig. 8 to examine the water wave interaction among cylinders. The calculation conditions are a_1=3.0m, b_1=1.0m, a_j=1.0m, b_j=0.5m (j=2,3,…,9) and d=20.0m. The ratio of depth is 0.5, the largest cylinder 1 is located at center, and the other cylinders are numbered clockwise from 2 to 9 shown in Fig 7. In the long wave region (ka≤0.7) the peak wave force of nine cylinders is largest and the difference of peak between seven cylinders and nine cylinders is small. The wave forces of nine cylinder gradually decreases and especially has a lower value than that of five cylinders in the short wave region(ka≥0.7). The difference between five cylinder and nine cylinders becomes larger as the wave number is greater than 0.7. It means that wave forces are strong influenced by the wave length and the water wave interaction is strongly depended on the relation between the wave length and the number of cylinders. Moreover, the hybrid substructure is significantly efficient to reduce the wave forces compared to substructure with mono pile in the short wave region.

The wave forces on each cylinder of hybrid substructure with seven and nine cylinders are shown in Fig. 9 and 10. The wave force on cylinder 1 is largest for all cases.

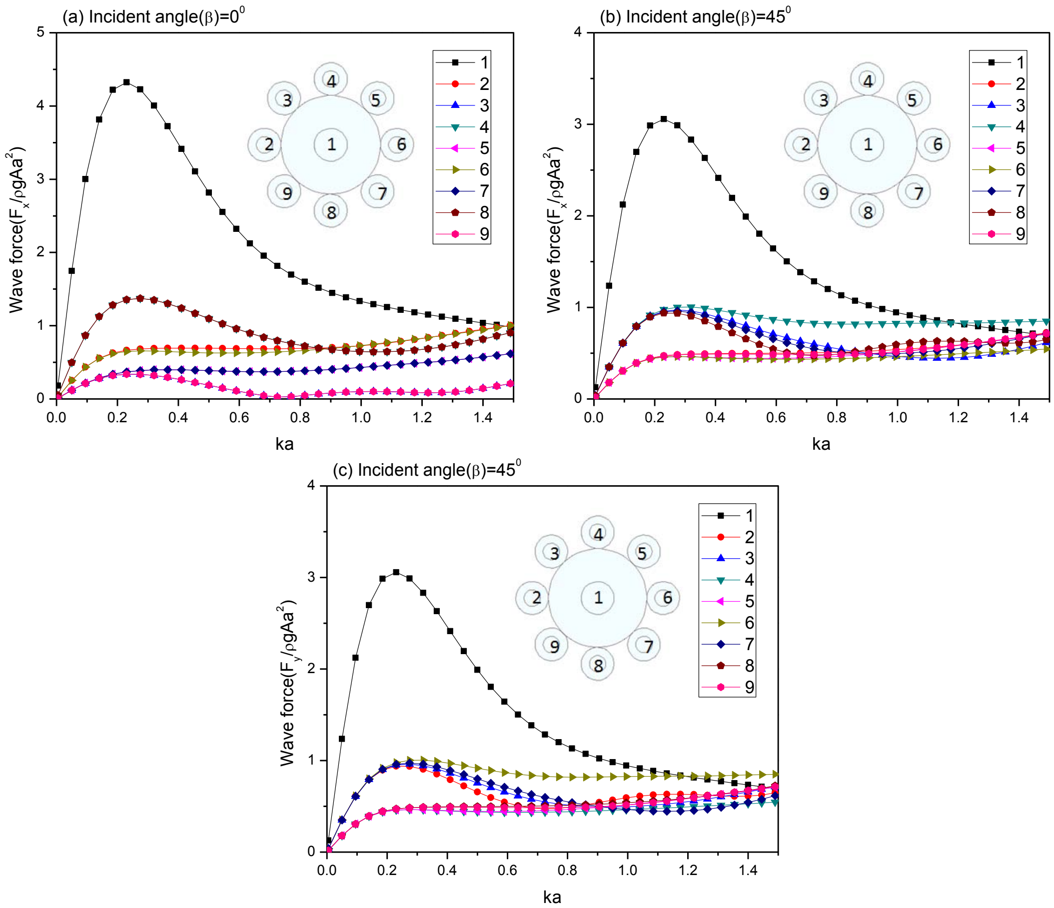

Fig. 10. Comparison of wave forces on each cylinder with a_1=3.0m, b_1=1.0m, a_j=1.0m, b_j=0.5m(j=2,3,…,9) and d=20.0m for various incident wave angles (β): (a) x-direction for β=0.0^0, (b) x-direction for β=45.0^0, (c) y-direction for β=45.0^0

Fig. 11 shows the comparison of wave run-up on each cylinder for various hybrid substructures. The wave run-up is normalized by incident wave height (H) and the abscissa denotes the angle(θ) measured counterclockwise from the positive x-axis. The cylinder 2 for both cases of five and nine cylinders has the similar pattern of wave run-up since the incident wave propagates toward the cylinder 2. The peak value of cylinder 1 is lowest in all cases. It is found that due to the reduction of wave-body interaction the wave run-up of cylinder 1 has a similar value regardless of the number of cylinders and the hybrid substructures, when the depth ratio of region 1 becomes a larger than 50.0% of whole water depth (*h/d*=0.5), is remarkably effective to reduce the wave run up.

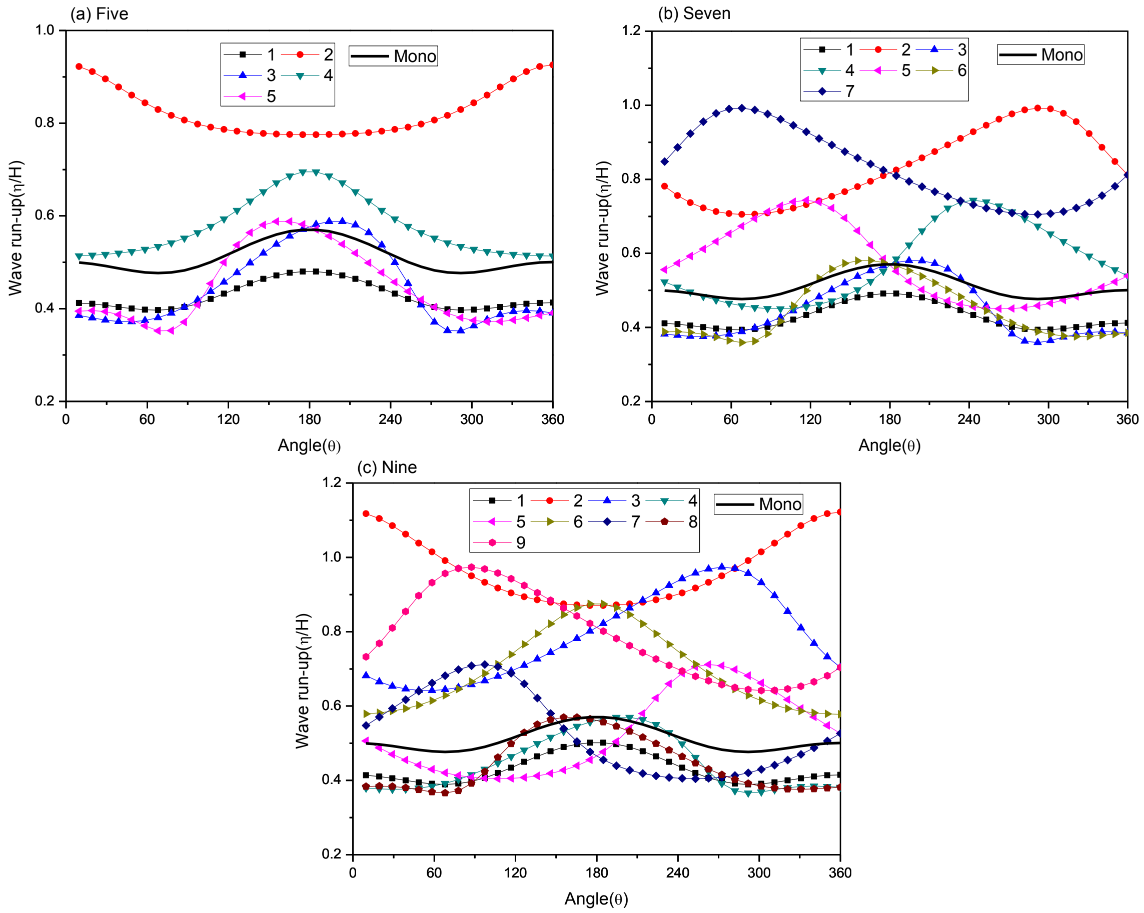

Fig. 11. Comparison of wave run-ups on hybrid substructure of various cylinder numbers with β=0.0^0, *h/d*=0.5 and *ka*=0.3: (a) Five cylinders, (b) Seven cylinders, (c) Nine cylinders

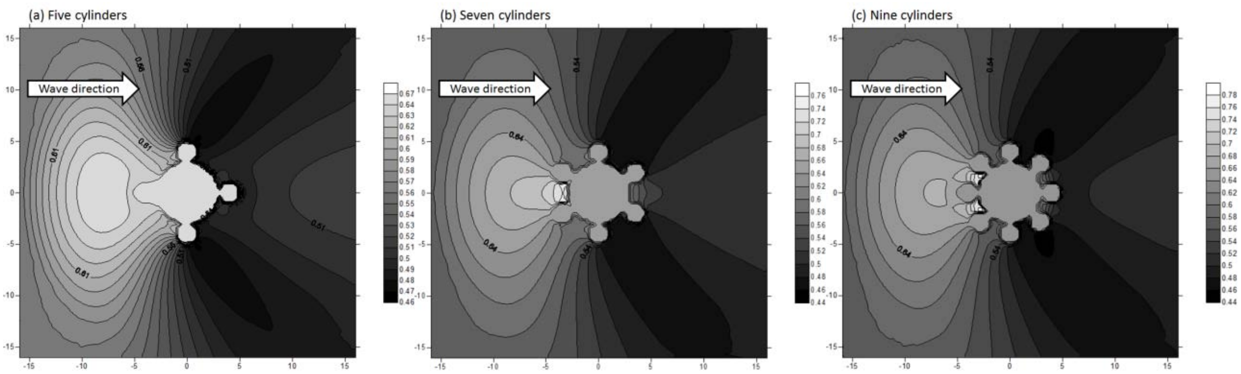

Fig. 12. Free surface elevation contours around hybrid substructure of various cylinder numbers with β=0.0^0, *h/d*=0.5 and *ka*=0.3: (a) Five cylinders, (b) Seven cylinders, (c) Nine cylinders

Fig. 12 shows the non-dimensional elevation contours on hybrid substructure of various cylinder members for wave number 0.3.

4. CONCLUSION

Hybrid substructure with multi-cylinders is newly suggested to reduce the wave forces on substructures. Under the assumption of potential flow and linear wave theory, a 3D numerical method for the hybrid substructure was developed using the Eigen-function expansion method. In the short wave region, the wave force on hybrid substructures is found to be greatly reduced compared to the case without small cylinder of region 1. Consequently, installing small cylinders of region 1 on the gravity substructure may be an effective means of decreasing the wave forces. It is also found that the hybrid substructure with depth ratio 0.25 of region 1 effectively reduces the wave force compared to the substructure with mono pile in the short wave region. Moreover the water wave interactions among cylinders rapidly diminish for the hybrid substructure. It means that the hybrid substructure significantly reduces the wave run-up on substructure. Consequently, the suggested hybrid substructure with multi-cylinders can be an effective substructure for reducing hydrodynamic effects in the short wave region.

ACKNOWLEDGEMENTS

This study was supported by the Korea Institute of Energy Technology Evaluation and Planning through the research project “Development of hybrid substructure systems for offshore wind power (2012T100201671)”.

REFERENCES

Abramowitz, M. and Stegun, I.A. (1972), “Handbook of Mathematical Functions”, Dover Publications, New York

Cho, I.H., and Kim, M.H. (2010). “Wave deformation and blocking performance by N porous bottom-mounted vertical circular cylinders.” *Int. J. Offshore and Polar Eng*. 20(4), 284-291.

Kagemoto, H., and Yue, D.K.P. (1986). “Interactions among multiple three-dimensional bodies in water waves; an exact algebraic method.” *J. Fluid Mech*. 166, 189-209.

Linton. C.M., and Evans. D.V. (1990). “The interaction of waves with arrays of vertical circular cylinder.” *J. Fluid Mech*. 215, 549-569.

McIver, P. (1984). “Wave forces on arrays of floating bodies.” *J. Engineering Math*. 18(4), 273-285.

McIver, P., and Evans, D.V. (1984). “Approximation of wave forces on cylinder arrays.” *Applied Ocean Res*. 6(2), 101-107.

Park, M.S., Koo, W.C., and Choi, Y.R. (2010). “Hydrodynamic interaction with an array of porous circular cylinders.” *Int. J. Naval Architecture and Ocean Eng*. 2(3), 146-154.

Spring, B.H., and Monkmeyer, P.L. (1974). “Interaction of plane waves with vertical cylinders.” *Proc. 14th International Conference on Coastal Engineering*, 107, 1828-1845.

Williams, A.N., and Abul-Azm, A.G. (1989). “Hydrodynamic interactions in floating cylinder arrays; Part II-Wave radiation.” *Ocean Eng*. 16(3), 217-264.
Williams, A.N., and Demirbilek, Z. (1988). “Hydrodynamic interactions in floating cylinder arrays; Part I-Wave scattering.” *Ocean Eng.* 15(6), 549-583.
Williams, A.N., and Li, W. (1998). “Wave interaction with a semi-porous cylindrical breakwater mounted on a storage tank.” *Ocean Eng*. 25(2-3), 195-219.
Williams, A.N., and Rangappa, T. (1994). “Approximate hydro-dynamic analysis of multi-column ocean structures.” *Ocean Eng*. 21(6), 519-573.
Zhao, F., Bao, W., Kinoshita, T., and Itakura, H. (2011). “Theoretical and experimental study on a porous cylinder floating in waves.” *J. Offshore Mechanics and Arctic Eng*. 133(1), 301-311.